JCI insight

Succinate dehydrogenase inversely regulates red cell distribution width and healthy lifespan in chronically hypoxic mice

Bora E. Baysal, … , Drew R. Jones, Sandra Sexton

JCI Insight. 2022. https://doi.org/10.1172/jci.insight.158737.

Research In-Press Preview Hematology Pulmonology

Graphical abstract

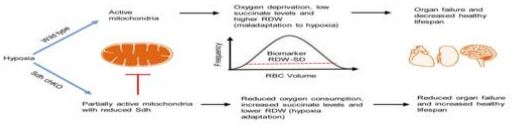

Succinate dehydrogenase inversely regulates red cell distribution width and healthy lifespan in chronically hypoxic mice

Bora E. Baysal[1@], Abdulrahman A. Alahmari[2,3], Tori C. Rodrick[4], Debra Tabaczynski[5], Leslie Curtin[6], Mukund Seshadri[7], Drew R. Jones[4], Sandra Sexton[6]

Departments of Pathology and Laboratory Medicine[1], Pharmacology and Therapeutics[2] Molecular and Cellular Biology[5] and Dentistry and Oral Oncology[7], Laboratory Animal Shared Resource[6], Roswell Park Comprehensive Cancer Center, Buffalo, New York 14263 USA. Department of Medical Laboratory Sciences[3], Prince Sattam Bin Abdulaziz University, Alkharj, Saudi Arabia. Metabolomics Core Resource Laboratory[4], NYU Langone Health, New York, NY 10016 USA

Conflict of interest: The authors have declared that no conflict of interest exists.

@ To whom correspondence should be addressed:

Bora E. Baysal MD, PhD

Department of Pathology and Laboratory Medicine

Roswell Park Comprehensive Cancer Center

Elm and Carlton Streets

Buffalo, NY 14263

Office:716-845-3204

Lab: 716-845-1197

Fax: 716-845-3427

Email: Bora. Baysal@roswellpark.org

Abstract

Increased red cell distribution width (RDW), which measures erythrocyte volume (MCV) variability (anisocytosis), has been linked to early mortality in many diseases and in older adults through unknown mechanisms. Hypoxic stress has been proposed as a potential mechanism. However, experimental models to investigate the link between increased RDW and reduced survival are lacking. Here, we show that lifelong hypobaric hypoxia (~10% O_2) increases erythrocyte numbers, hemoglobin and RDW, while reducing longevity in male mice. Compound heterozygous knockout (chKO) mutations in succinate dehydrogenase (Sdh; mitochondrial complex II) genes *Sdhb*, *Sdhc* and *Sdhd* reduce Sdh subunit protein levels, RDW, and increase healthy lifespan compared to wild-type (WT) mice in chronic hypoxia. RDW-SD, a direct measure of MCV variability, and the standard deviation of MCV (1SD-RDW) show the most statistically significant reductions in Sdh hKO mice. Tissue metabolomic profiling of 147 common metabolites shows the largest increase in succinate with elevated succinate to fumarate and succinate to oxoglutarate (2-ketoglutarate) ratios in Sdh hKO mice. These results demonstrate that mitochondrial complex II level is an underlying determinant of both RDW and healthy lifespan in hypoxia, and suggest that therapeutic targeting of Sdh might reduce high RDW-associated clinical mortality in hypoxic diseases.

Key Words: Hypoxia**,** mitochondria, biomarker, complete blood count (CBC), mortality, complex II, RDW

Introduction

Erythrocyte anisocytosis refers to increased variation in red blood cell (RBC) volume, and is measured by red cell distribution width (RDW) in routine complete blood count (CBC) analysis. RDW is often reported as a coefficient of variation (RDW-CV) of erythrocyte mean corpuscular volume (MCV) in RBC volume distribution curve. RDW-CV is calculated by dividing the standard deviation (1SD-RDW) by MCV, multiplied by 100. RDW-SD is a direct measure of anisocytosis that reports the MCV variation at 20% frequency level (1). RDW increases in healthy aging population (2).

RDW along with MCV is traditionally used in the differential diagnosis of anemia. In recent years, however, high RDW has been associated with increased mortality in acute and chronic diseases as well as in middle-aged and older individuals without disease (3, 4). The association has been observed in a growing list of clinical conditions including heart failure (5, 6), myocardial infarction (7), peripheral artery disease (8), cancer (9), pulmonary hypertension (10), acute pulmonary embolism (11), community-acquired pneumonia (12, 13), SARS-CoV-2 infection (14), chronic obstructive pulmonary disease (15, 16), acute respiratory distress syndrome (17), acute cerebral infarction and stroke (18, 19), intensive care unit (ICU) and trauma patients (20-22), hip fracture (23), sepsis and septic shock (24), gram-negative bacteremia (25), acute pancreatitis (26), hemodialysis (27), and kidney transplant receivers (28). The underlying mechanisms that contribute to increased mortality in the context of increased RDW is unknown.

Although anisocytosis is a physiologic response to anemia, the association with mortality remains significant in non-anemic individuals (7, 29-34), and becomes even stronger in non-anemic individuals than in anemic ones in meta-analysis (35). A correlation between inflammatory markers and anisocytosis has been documented, which raises the hypothesis that the effect of RDW on mortality may be mediated by systemic inflammation (36). However, the

association of anisocytosis with mortality and disease remains statistically significant even in subjects with low CRP levels, a marker of inflammation (4, 37, 38). It has been hypothesized that RBCs with increased size variation may have reduced deformability that impairs micro-circulatory blood flow, though contrasting results were reported on the impact of increased RDW on RBC deformability (39, 40). Furthermore, certain anemias cause marked anisocytosis without significantly increasing the mortality risk. For example, dietary iron deficiency anemia is attributed to ~0.08 deaths per 100,000 (41). These considerations collectively suggest that the mortality risk associated with anisocytosis cannot be readily explained by anemia, inflammation or RBC physicochemical characteristics.

Increased anisocytosis may reflect a fundamental cellular pathology that predisposes to mortality regardless of the specific clinical condition. Yčas et al. analyzed over 2 million medical claims and concluded that RDW indicates systemic hypoxic load, especially in pulmonary and cardiac conditions (42). High RDW correlates with severity and poor survival in COPD (15, 16, 43, 44) as well as with lung function in normal subjects (45). A recent analysis of RDW in 121,530 non-anemic individuals with a medical condition revealed the strongest associations with pulmonary hypertension, chronic pulmonary heart disease and congestive heart failure, which all have a pathophysiologic link to hypoxia (46). Similarly both hypoxemia and high RDW have been linked to mortality risk in COVID-19 patients (14, 47). Hypoxia triggers the production of RBC precursor reticulocytes from bone marrow through the operation of PhD-HIF pathway that regulates the erythropoietin production(48). Since reticulocytes are larger than mature RBCs, anisocytosis ensues. Thus, systemic hypoxia appears to be a biologically plausible stress factor that might explain the association between anisocytosis and mortality. However, experimental evidence for this hypothesis is lacking.

In this study, we report on the impact of chronic hypobaric hypoxia on RBC parameters and healthy lifespan in Sdh heterozygous and wild-type (WT) control male mice. In humans,

heterozygous germline SDH subunit mutations predispose to paraganglioma (PGL) and pheochromocytoma tumors (49). Hereditary PGL tumors caused by *SDHD* mutations often develop in the carotid body (CB) in neck (50), and mimic the sporadic CB paragangliomas caused by chronic hypoxic stimulation of high altitudes (51). Higher altitude increases the severity of hereditary PGL tumors (52, 53). Gene expression profiling studies in SDH PGLs show persistent activation of hypoxia-induced genes in normoxic conditions (pseudo-hypoxia)(54). These results collectively suggest that SDH mutations predispose to PGL tumors by constitutively activating the hypoxia-sensing/signaling pathways in paraganglionic tissues.

Sdh mouse models show that while homozygous deficiency of a subunit is incompatible with normal life and development, heterozygous mutations do not cause paraganglioma tumors (55-57). Here, we present evidence that chronic hypoxic stimulation also fails to develop paraganglioma tumors in Sdh mice. Unexpectedly, we find that mice with partial Sdh deficiency show reduced RDW and increased healthy lifespan relative to control mice in chronic hypoxia, revealing a mechanism contributing to the association between high RDW and mortality.

Results

Sdh knockout mice

The experimental mice were derived by crossing the three previously described original strains each containing a heterozygous knockout (hKO) mutation in *Sdhb, Sdhc* or *Sdhd* (See Methods)(58). Genotypes were determined by gene KO-specific PCR amplifications from tail DNA. To confirm that hKOs reduce complex II protein levels, we performed western blot analysis in WT (n=3), *Sdhb* single hKO (n=3), *Sdhb/c* double hKO (n=3) and *Sdhb/c/d* triple hKO (n=3) male mice using heart, kidney and brain tissues (**Figure 1A and Supplemental Figure 1**). We first evaluated linearity in dose-response relationship in western blots

(**Supplemental Figure 2)**. Sdhb and Sdhc protein levels quantified against the control complex I protein NDUFB8 showed statistically significant reductions in single or compound hKO mice (**Figure 1B**). Notably, Sdhc protein levels were also decreased in Sdhb and Sdhb/d mice in kidney and brain. Also, Sdhb protein levels were less in Sdhb/d and Sdhb/c/d than in Sdhb mice in heart and kidney. These results suggest that individual subunit levels decrease further by reductions in other subunits, possibly through degradation of the unincorporated proteins into complex II. These findings are consistent with the observations that immunohistochemical loss of *SDHB* in paragangliomas can occur with inactivating mutations in *SDHA, SDHB, SDHC, SDHD*, or *SDHAF2* subunit genes (59).

Sdh heterozygous knockout mice do not develop tumors under chronic hypoxia.

The development of PGL or other tumors was prospectively examined in 3 sequentially tested groups of male mice exposed to lifelong hypoxia (~10% O_2). Group 1 had Sdh double hKO of *Sdhb/c*, whereas Groups 2 and 3 had Sdh triple hKO of *Sdhb/c/d* **(Table 1)**. The initial goal was to determine whether compound heterozygosity in Sdh predisposes to PGL tumor development under chronic hypoxia. Non-invasive magnetic resonance imaging (MRI) analysis of chKO *Sdhb/c* (mouse #145) and WT control (mouse #197) mice after ~7 months of chronic hypoxia exposure showed no radiologic evidence of tumor development in either genotype (**Supplemental Figure 3**). Gross and microscopic examination of the hypoxia-exposed mice confirmed lack of tumor development or vascular pathology such as intimal thickening or plexiform lesions in lung or pheochromocytoma development in adrenal gland (**Supplemental Figure 4**). Thus, although hypobaric hypoxia of high altitudes has been shown to promote development of sporadic paragangliomas in humans (60), we found no evidence of Sdh-related PGL tumor development in mice in normoxia or following exposure to chronic hypoxia.

Sdh heterozygous knockout mice survive longer under chronic hypoxia.

We observed 3 sequential groups of chKO and WT control male mice until spontaneous death or development of morbidities that require euthanasia (i.e., healthy lifespan). WT control mice were of similar age and selected from the same or closely related litters. Healthy lifespans of mice in chronic hypoxia (median 503 days for Sdh chKO and 456 days for WT control) were substantially lower than that of the parental B6 mice living in room conditions (~ 2.5 years). However, we found that Sdh chKO mice survived longer than WT control mice in each of the 3 experimental groups (**Table 1**). When data from 3 groups were combined, the lifespan differences between Sdh chKO and WT mice were statistically significant (P<0.0001 by Log-rank (Mantel-Cox) test and P=0.0024 by Gehan-Breslow-Wilcoxon test. **Figure2**). The rate of hypoxic death/moribund conditions in WT mice, estimated by Hazard ratio, was 11.39 (95% CI of 3.419 to 37.95) and 4.65 (95% CI of 1.606 to 13.47) fold higher than Sdh chKO mice by Mantel-Haenszel and logrank methods, respectively. Four WT mice and 1 *Sdhb/c* mice were euthanized based on institutional guidelines due to the development of morbid conditions. The survival difference between Sdh chKO (n=6) and WT (n=7) mice was statistically significant even when the mice euthanized for moribund conditions were excluded from the analysis (P=0.0037 Log-rank (Mantel-Cox) test and P=0.0304 Gehan-Breslow-Wilcoxon test).

Necropsy of mice revealed no specific causes to explain early death or the development of moribund conditions, but showed congestion and enlargement of spleen and heart which are expected under chronic hypoxia. Chronic hypoxia is associated with the development of pulmonary hypertension and right ventricular hypertrophy. We assessed right ventricular hypertrophy by Fulton index in experimental group 2, and found no statistically significant differences between Sdh and WT control mice (**Supplemental Figure 5**). This result suggests that pulmonary hypertension differences do not probably explain the differential survival between the Sdh chKO and WT mice.

Sdh hKO mice show evidence of reduced RBC regeneration and lower red cell distribution width (RDW)

To examine whether erythrocyte numbers could explain the survival differences between the two genotypes, we analyzed CBC variables from 3 groups of Sdh hKO male mice and WT controls using 2way ANOVA test. No statistically significant differences were observed in RBC numbers or hemoglobin (HGB) levels in any group (**Figure 3**). Reduced hematocrit (HCT) (**Figure 3**), mean corpuscle volume (MCV), mean corpuscular hemoglobin (MCH) (**Figure 3**), RDW-CV (**Figure 4**), reticulocyte percentage (Ret %, **Figure 4**) and immature reticulocyte fraction (IRF) (**Figure 3**) were observed in Sdh chKO mice in 1 of 3 groups. The most statistically significant difference between the genotypes were observed in direct measures of RBC size variability, namely RDW-SD and 1SD-RDW which showed a reduction in Sdh chKO mice in 2 of 3 groups (**Figure 4**).

Analysis of the combined data from all 3 groups showed the most statistically significant differences in RDW-SD, RDW-CV, 1SD-RDW and IRF both in normoxia and hypoxia with lower values observed in Sdh chKO mice relative to WT control mice (**Table 2**). Borderline statistically significant differences were seen in hematocrit and MCV in hypoxia and reticulocyte percentage in normoxia. No statistically significant differences were seen in the numbers of white blood cells, platelets and in platelet distribution width (PDW) between Sdh hKO and WT mice in normoxia or hypoxia (**Figure 4** and **Table 2**). Collectively, the differences in RBC parameters reveal blunted rate of erythropoietic activity and erythrocyte regeneration by partial loss of Sdh, especially in hypoxia.

Metabolomic analysis shows increased succinate levels, and succinate:fumarate and oxoglutarate ratios in Sdh hKO mice

To examine metabolic differences between Sdh hKO mice (n=3 Sdhd and n=5 Sdhb/c/d) and WT (n=2) mice, we obtained metabolic profiles of liver, skin, kidney, heart and brain by quantifying 147 common metabolites **(Supplemental Table 2)**. A principle component analysis (PCA) showed distinct clustering amongst each tissue type, with the heart samples and the brain samples grouping closely together, irrespective of the genotype (**Supplemental Figure 6**). We ranked the metabolites by the average of their log2FoldChange between genotypes across five tissues and examined the extreme outlier metabolites that do not fit to a Gaussian distribution using ROUT method and false discovery rate of Q=0.1% (61). Succinate was the only outlier metabolite identified in both Sdhd and Sdhb/c/d hKO mice (**Figure 5A**). Glycerol 3-phosphate, xanthylic acid and adenosine diphosphate ribose were also identified as increased outliers in Sdhb/c/d hKO mice, but not in Sdhd mice. Succinate increased by 2.9-fold and 4.02-fold in Sdhd and Sdhb/c/d hKO mice, respectively, leading to increased ratios of succinate to fumarate and oxoglutarate (2-ketoglutarate) (**Figure 5B**). The most decreased metabolites commonly detected in both hKO genotypes were 3-hydroxybutyrate and L-cystine, which decreased by more than 1.5-fold but less than 2-fold (**Figure 5A**). Neither metabolite was identified as an outlier by the ROUT method.

Discussion

In this study, we show that chKO mutations in Sdh genes prolong healthy lifespan by ~10% under chronic hypoxia and reduce multiple measures of RBC anisocytosis including RDW-SD, RDW-CV and 1SD-RDW. Other parameters related to RBC regeneration including IRF, HCT and MCV also show evidence of reductions in Sdh KO mice compared to WT. The lack of statistically significant differences in RBC numbers or HGB suggest that Sdh regulates the rate of hypoxia-dependent RBC regeneration, but not the total RBC or hemoglobin levels. We find

no evidence of PGL tumor development in mice even with chronic lifelong hypoxia exposure, in agreement with a recent study (57). These findings collectively show a previously unrecognized role for Sdh in regulation of erythroid regeneration both in normoxia and hypoxia. To our knowledge, this is also the first mammalian study showing a hypoxia-survival benefit upon partial constitutional loss of Sdh. Our findings parallel those observed in other organisms.

Studies in *Ascaris Suum*, a helminthic parasite, show that Sdh is active in spore forms which respire atmospheric O_2, but not in the adult forms which live in the hypoxic environment of the host intestine. The adult parasite instead uses fumarate reductase (Frd), which catalyzes the reverse reaction of Sdh (62). A hypoxic switch in Sdh genes controls respiration in *Mycobacterium Tuberculosis* (63). ATP producing eukaryotic mitochondria use Frd rather than Sdh under limited O_2 conditions (64). Flies resistant to hypoxia have reduced complex II activity levels compared to the control flies (65). Anoxic environments (N_2 or CO_2) lead to decreased transcript expression of the 3 of four SDH subunit genes, by promoter methylation in maize (66). Furthermore, suppressing mitochondrial respiration was found to be promote hypoxia tolerance in fetal growth plate (67). Our findings combined with these studies suggest that inhibition of Sdh is a universal theme in organismal adaptation to hypoxia/anoxia across diverse organisms including mammals.

Identification of the molecular mechanisms linking reduced Sdh to organismal tolerance to hypoxia requires further studies. There is, however, existing evidence that loss of SDH triggers hypoxia adaptation pathways in human PGL tumors(54). Several studies have shown increased succinate to fumarate and succinate to oxoglutarate ratios in SDH-mutated PGL tumors. Increased succinate relative to oxoglutarate inhibits α-ketoglutarate dependent enzymes

including HIF prolylhydroxylases (68), Jumonji domain histone demethylases (69) and TET family of 5-methyldeoxycytosine hydroxylases (70), contributing to pseudohypoxia and hypermethylation in PGL tumors. We also find increased succinate to fumarate and succinate to oxoglutarate ratios in tissues from Sdh hKO mice, even though global tissue-specific metabolite profiles were not drastically altered by partial Sdh loss. In contrast to expectations that Sdh partial loss could further enhance erythropoiesis by succinate-mediated inhibition of HIF prolylhydroxylases, leading to HIFα stabilization, we see evidence of *reduced* erythropoiesis. This finding suggests that increased intracellular oxygen availability upon partial loss of Sdh plays a more dominant role in HIFα regulation by promoting HIF prolylhydroxylase activity than the inhibitory impact of increased succinate levels. It is conceivable that alterations in succinate, 3-hydroxybutyrate and L-cystine or other metabolite levels contribute to systemic hypoxia tolerance and increased healthy lifespan in Sdh hKO mice. The *SDHD* gene is subject to maternal imprinting (inactivation) in hypoxia-sensitive carotid body chief cells, because only a paternal transmission, but not maternal transmission, of the mutated *SDHD* gene predisposes to paraganglioma tumors. Thus, partial loss of SDH activity by genomic imprinting might facilitate hypoxia sensing and/or adaptation in carotid body cells (71). We recently showed that pharmacologic inhibition of complex II by atpenin A5 triggers hypoxic gene expression and RNA editing by APOBEC3A and APOBEC3G cytidine deaminases independently of HIF1 in monocytes and natural killer (NK) cells, respectively (58, 72). The *SDHB* and *SDHA* genes acquire nonsense/missense RNA editing by APOBEC3A in monocytes subjected to cellular crowding and hypoxia (73, 74). RNA editing by APOBEC3G in NK cells is induced by cellular crowding and hypoxia and promotes Warburg-like metabolic remodeling by suppressing O_2 consumption relative to glycolysis (72). It is conceivable that the inhibition of Sdh in mice activates similar HIF-independent hypoxia-adaptation pathways including gene expression, RNA editing and possibly other adaptive pathways that remain to be discovered.

Importantly, our findings suggest a mitochondrial basis for the association between high RDW and mortality observed in many diseases. Previous research has established that inhibition of mitochondrial respiration antagonizes the hypoxic stabilization of HIF-α (75, 76), the key molecular event driving the synthesis of erythropoietin that stimulates RBC regeneration in bone marrow. Pharmacologic inhibition of complex II by atpenin A5 reduces the stabilization of HIF-α in cancer cell lines in hypoxia, and reduces baseline O_2 consumption (58, 77). Atpenin A5 is a highly potent complex II inhibitor of ubiquinone binding at the interface of Sdhb, Sdhc and Sdhd subunits (78, 79). Therefore, we suggest that partial loss of Sdh in hKO mice reduces mitochondrial O_2 consumption, and leads to blunted HIF-mediated RBC regeneration and RDW in hypoxia.

Jain et al (80) found that hypoxia and inhibition of VHL, which triggers HIF-mediated cellular hypoxia response, promote survival in a genetic mouse model with mitochondrial respiratory defect, and in cell culture and zebrafish models, respectively. Although the exact mechanisms are unclear, normal O_2 levels seem detrimental when mitochondrial respiration is impaired. Our model suggests that the opposite is also true: reduced O_2 levels are detrimental when the mitochondrial respiration is intact. Therefore, it appears that optimum organismal survival requires a balance between mitochondrial activity levels and O_2 abundance and that Sdh levels play an important role in hypoxic survival.

Our study has certain limitations including the lack of a specific disease model in which high RDW has been associated with early mortality in clinical studies, and the indeterminate causes of death in hypoxic mice. Also, these findings are obtained only in male mice and remain to be extended to female mice. Further studies are required to close these knowledge gaps in the future.

In summary, our findings show that Sdh plays an unanticipated role in regenerative erythrocyte anisocytosis and organismal lifespan in mice under chronic hypoxia. These results support a model that upon systemic hypoxia, mitochondrial O_2 consumption depletes cellular O_2, leading to cellular injury, organ failure and death while increasing RDW through HIF-dependent erythropoiesis. Suppressing Sdh reduces O_2 consumption, mitigates cellular hypoxia, blunts RDW and triggers HIF-independent hypoxia adaptation pathways to promote organismal tolerance to chronic hypoxia **(Figure 6)**. Direct testing of tissue O_2 consumption rates in Sdh mice remains to be performed, although we and others reported diminished mitochondrial O_2 consumption upon Sdh inhibition by atpenin A5 in mammalian cells (58, 77). We hypothesize that high RDW is merely a surrogate biomarker for cellular hypoxia which is controlled in part by mitochondrial O_2 consumption, and that hypoxia is the ultimate driver of cell death, organ failure and mortality. Therefore, therapeutic targeting of Sdh may reduce high RDW-associated mortality in hypoxic diseases by enhancing systemic adaptation to hypoxia.

Methods

Sdh knockout mice:

Sdhb and *Sdhc* heterozygous KO mice were created in The Jackson Laboratory (Bar Harbor, Maine) in B6/129P2 background and described as: B6.129P2-Sdhb<Gt(AP0532)Wtsi>/Cx and B6.129P2-Sdhc<Gt(BA0521)Wtsi>/Cx. (58). The *Sdhd* knockout mouse (81) was re-derived into C57BL/6J background at RPCCC transgenic facilities using frozen sperm (mfd Diagnostics, Germany). As previously reported, homozygous mutations in any subunit are non-viable, but compound *Sdhb/Sdhc* double heterozygous and *Sdhb/Shdc/Sdhd* triple heterozygous KO mice are viable (58). Since each gene is located on a different mouse chromosome, the KO alleles segregate independently and give the expected numbers of each viable genotype upon crossing the Sdh hKO mice. Control WT mice were also derived from crosses of Sdh hKO mice. WT controls in hypoxia experiments were either littermates or from closely related litters. Genotyping was performed in tail tips at RPCCC transgenic facility as described (58). Genotypes of the mice in hypoxia chamber are confirmed by repeat testing.

Hypoxia exposure:

Mice were exposed to chronic hypobaric hypoxia in a custom-made hypoxia chamber (Case Western Reserve University Design Fabrication Center, Cleveland, OH) that operates via house vacuum and accommodates 2 standard mice cages (5 mice per cage), as previously described (58). Mice were initially subjected mild hypoxia (~14% O_2) for ~1 week for acclimatization. For chronic exposure, the oxygen concentration was ~10% with a range of 9–11%. Oxygen percentage is continuously monitored by an O_2 sensor. Hypoxia exposure experiments involved 5 compound heterozygous and 5 WT control mice (~ 10 weeks of age), with each genotypic group placed in a different cage. Mice were daily observed, and briefly removed from the chamber twice a week for cage cleaning.

Mice remained in hypoxia chamber until spontaneous death or the development of morbid conditions, as assessed during cage cleaning, that required euthanasia in accordance with Roswell animal care guidelines and the approved IACUC protocol. Examples of morbid conditions included limited or absent movement, hunched posture, labored breathing, sunken eyes, shaking and development of rectal prolapse. All decisions for euthanasia due to morbid status were made in accordance with approved IACUC guidelines. Organs were grossly examined during necropsy. Tissues were collected upon spontaneous death and euthanasia.

Peripheral blood analysis:

Body weights were measured, and blood was collected for CBC analysis. Blood (~0.2 mL) is collected into EDTA tubes by retro-orbital bleeding at baseline and subsequent time points. Alternate eyes were used for a maximum of 2 times per eye. Additional bleeding was performed by mandibular venipuncture. Complete blood counts were analyzed via automated cell counters Hemagen HC5 (first 2 time points in Group 1) or ProCyte Dx (the third time point in Group 1, Groups 2 and 3) hematology analyzers available at Roswell Laboratory Animal Shared Resources. Certain RBC parameters such as RDW-SD, Ret% and IRF were not reported by Hemagen HC5 counter. The RBC parameter values examined in this study are direct outputs of the analyzers except 1SD-RDW, which is derived as (RDW-CVXMCV)/100.

Subcellular fractionation:

Mitochondria were isolated from mouse tissues by homogenization and centrifugation. Briefly, fresh frozen tissues were thawed in homogenization buffer (20 mM HEPES, pH 7.4; 10 mM KCl; 1.5 mM MgCl2; 1 mM EDTA; 1 mM EGTA; 250 mM sucrose) supplemented with freshly added 1X protease inhibitor cocktail and 1 mM DTT. 1 ml of homogenization buffer was used per 100 mg tissue. Tissues were chopped as much as possible using a fine pointed scissor in the homogenization buffer and incubated for 30 min in ice with intermittent vortexing. Tissues were then homogenized using a dounce homogenizer (~35-40 strokes using loose pestle) and pre-

cleared of debris using centrifugation at 1000g for 10 min. Supernatant was collected in new tube and centrifuged at 12000 rpm for 20 min to obtain a mitochondrial pellet. Supernatant was collected as cytosolic fraction, and mitochondrial pellets were washed 4 times with homogenization buffer. Mitochondrial pellets were lysed in RIPA buffer and assayed as the mitochondrial fraction.

Western blotting:

Cytoplasmic and mitochondrial lysates were mixed in Laemmli buffer, denaturized for 5 min at 95°C and 55°C, respectively, and run on 15% SDS-PAGE. Proteins were then transferred to nitrocellulose membranes (0.2 µm, Bio-Rad, Cat. # 1620112) at a constant voltage of 100V for 70 min at 4°C using Mini Trans-Blot® Cell (Bio-Rad). Membranes were incubated in Tris-buffered saline (TBS) with 0.1% v/v TWEEN-20 (Sigma Aldrich) and 5% w/v nonfat dry milk (Blotting-Grade Blocker #1706404, Bio-Rad). Primary antibodies were diluted in 3% BSA in TBS with 0.1% TWEEN-20 and applied to the nitrocellulose membrane as follows: mouse anti-Total OXPHOS Rodent Antibody Cocktail (Abcam, product number ab110413, 1:1000 dilution), Rabbit polyclonal anti-SDHC Polyclonal Antibody (ThermoFisher Scientific, product number 14575-1-AP, 1:500 dilution). For secondary antibodies, horseradish peroxidase-conjugated, Donkey anti-rabbit (Fisher Scientific, Catalog number: 45-000-682) or Goat anti-mouse (Sigma-Aldrich, Catalog number: A4416) IgG antibodies were used at 1:2,000 dilution. Pierce ECL Western Blotting Substrate (Thermo Scientific, Catalog number: 32106) was used for chemiluminescent detection. Signals were visualized and imaged using the ChemiDoc XRS+ System and Image Lab Software (Bio-Rad). Protein quantification was performed using ImageJ software (ImageJ, U. S. National Institutes of Health) by measuring bands intensity. To evaluate linear signal-response relationship in western blots, one sample from each genotype group, was loaded in three different concentrations of each (2.5, 5 and 10 µg). We probed for OXPHOS and Sdhc, quantified the signals and plotted them individually for linearity. This experiment showed

expected directionality in 35 of 36 signal intensity comparisons, except for Sdhc WT 2.5 vs 5 µg comparison (Supplemental Figure 2).

Magnetic Resonance Imaging:

Experimental magnetic resonance imaging (MRI) examination was performed using a 4.7 T/33-cm horizontal bore magnet (GE NMR Instruments, Fremont, Calif) within the Translational Imaging Shared Resource at Roswell Park Comprehensive Cancer Center. Preliminary scout images were acquired on the sagittal plane for localization and for determination of subsequent slice prescriptions. Coronal T2-weighted (T2W) images were acquired using protocols previously described by us (82, 83).

Metabolomic extraction and analysis

Tissues (liver, kidney, heart, skin and brain) from 10 mice (2 WT, 3 *Sdhd* single hKO and 5 *Sdhb/c/d* triple hKO) were assayed for glycolytic and tricarboxylic acid (TCA) cycle intermediates at NYU Langone's Metabolomics Laboratory. Samples were analyzed-by liquid chromatography-mass spectrometry (LCMS) assay after scaling the metabolite extraction to a measured aliquot. Each of the 50 frozen samples were weighed on an analytical balance and then extracted in-80% methanol buffer on dry ice containing 500 nM of labelled amino acid internal standards, using a ratio of 10 mg tissue per mL of extraction solution. Samples were homogenized in a BeadBlaster™ using ~100 µL of zircon beads (0.5 mm), centrifuged (21,000xg for 3 min), and then 450 µL of the supernatant was dried down by speed vacuum concentration and reconstituted in 50 µL of LCMS grade water. Reconstituted samples were sonicated for 2 minutes and then transferred into LCMS vials with glass inserts.

LC-MS/MS with the hybrid metabolomics method

Samples were subjected to an LCMS analysis to detect and quantify known peaks. Intensities were extracted with an in-house script with a 10 ppm tolerance for the theoretical *m*/*z* of each metabolite, and a maximum 30 sec retention time window. A metabolite extraction was carried out on each sample based on a previously described method (84). The LC column was a Millipore™ ZIC-pHILIC (2.1 x150 mm, 5 µm) coupled to a Dionex Ultimate 3000TM system and the column oven temperature was set to 25°C for the gradient elution. A flow rate of 100 µL/min was used with the following buffers: A) 10 mM ammonium carbonate in water, pH 9.0, and B) neat acetonitrile. The gradient profile was as follows; 80-20%B (0-30 min), 20-80%B (30-31 min), 80-80%B (31-42 min). Injection volume was set to 2 µL for all analyses (42 min total run time per injection).

MS analyses were carried out by coupling the LC system to a Thermo Q Exactive HF™ mass spectrometer operating in heated electrospray ionization mode (HESI). Method duration was 30 min with a polarity switching data-dependent Top 5 method for both positive and negative modes. Spray voltage for both positive and negative modes was 3.5kV and capillary temperature was set to 320°C with a sheath gas rate of 35, aux gas of 10, and max spray current of 100 µA. The full MS scan for both polarities utilized 120,000 resolution with an AGC target of 3e6 and a maximum IT of 100 ms, and the scan range was from 67-1000 m/z. Tandem MS spectra for both positive and negative mode used a resolution of 15,000, AGC target of 1e5, maximum IT of 50 ms, isolation window of 0.4 *m*/*z*, isolation offset of 0.1 *m*/*z*, fixed first mass of 50 m/z, and 3-way multiplexed normalized collision energies (nCE) of 10, 35, 80. The minimum AGC target was 1e4 with an intensity threshold of 2e5. All data were acquired in profile mode.

Relative quantification of metabolites

The resulting Thermo™ RAW files were read using ReAdW.exe version 4.3.1 to enable peak detection and quantification. The centroided data were searched using an in-house python script Skeleton version 4.0 and peak heights were extracted from the raw files based on a

previously established library of metabolite retention times and accurate masses adapted from the Whitehead Institute (84), and verified with authentic standards and/or high resolution MS/MS spectral manually curated against the NIST14MS/MS (85) and METLIN (2017) (86) tandem mass spectral libraries. Metabolite peaks were extracted based on the theoretical *m/z* of the expected ion type e.g., $[M+H]^+$, with a ±5 part-per-million (ppm) tolerance, and a ± 7.5 second peak apex retention time tolerance within an initial retention time search window of ± 0.5 min across the study samples. The resulting data matrix of metabolite intensities for all samples and blank controls was processed with an in-house statistical pipeline Metabolyze version 1.0 and final peak detection was calculated based on a signal to noise ratio (S/N) of 3X compared to blank controls, with a floor of 10,000 (arbitrary units). For samples where the peak intensity was lower than the blank threshold, metabolites were annotated as not detected, and the threshold value was imputed for any statistical comparisons to enable an estimate of the fold change as applicable. The resulting blank corrected data matrix was then used for all group-wise comparisons, and t-tests were performed with the Python SciPy (1.1.0) (87) library to test for differences and generate statistics for downstream analyses, unless otherwise specified. Any metabolite with p-value < 0.05 was considered significantly regulated (up or down). Heatmaps were generated with hierarchical clustering performed on the imputed matrix values utilizing the R library pheatmap (1.0.12) (88). Volcano plots were generated utilizing the R library, Manhattanly (0.2.0).

Statistics:

Statistical analysis and graphic presentations are performed by GraphPad Prism (Versions 7.03 and 9.2.0). P values of less than 0.05 (two-tailed) were considered statistically significant. Band intensities in western blots is compared by ordinary one-way ANOVA. Since limited preplanned comparisons were made in band intensities, corrections for multiple comparisons were not

performed. CBC output values are first entered to Microsoft Excel and then imported into GraphPad. The full CBC dataset used in analyses are provided as Supplemental Table 1. A few extreme outlier CBC values (9 of 1393=~0.65%) were removed by ROUT method. The comparisons of CBC values over time between Sdh chKO and WT controls were performed by 2-way ANOVA test by using data from all available time points, including the baseline normoxic values, within each experimental group. The independent variables are time and genotype. The data is arranged so that each row represents a different time point and matched values from each mouse are stacked in a subcolumn. Two-way ANOVA tests were performed to test the main effects only (time and genotype). Since erythrocytosis is a well-known response to chronic hypoxia, we only report genotype differences. As implemented in GraphPad Prism, we used Geisser-Greenhouse correction (i.e., sphericity or equal variability of differences was not assumed). When there were no missing data, repeated measures ANOVA was used. However, since most of the analyzed data sets contained random missing values (due to loss of mice, technical errors in CBC analysis or outlier removal), mixed-effects model was used since repeated measures ANOVA requires no missing values. When the genotype comparison was made in normoxia or hypoxia, data from all time points from all three groups were combined, and ordinary two-way ANOVA was used. P values that remain significant (less than 0.05) after adjustment for multiple comparisons by Holm-Šídák method (alpha:0.05) are indicated in Figures 3, 4 and Table 2. The survival differences were calculated by Kaplan-Meier method, where the outcome is time until death or the development of morbid conditions that required euthanasia. Outlier detections in CBC and average of log2FoldChange in 5 tissues in metabolomics data were performed using the most stringent criteria of GraphPad's ROUT method, which is Q=0.1% (i.e., no more than 0.1% of the identified outliers are false).

Study approval

All experimental and mice protocols are approved by Roswell Park Cancer Institute IACUC.

Author Contributions

BEB designed the study with contributions from DT, SS and DRJ. AAA performed Western blot analysis and prepared Figure 1. TCR and DRJ performed the metabolomics study. DT performed mice handling, care, identification and breeding. DT, SS and LC performed mice physical evaluations, blood draws and necropsy. MS performed MRI analysis. BEB performed the stastitical analysis, prepared the remaining figures and wrote the manuscript with contributions from AAA and DRJ. All authors reviewed the manuscript and agreed on the authorship.

Acknowledgements

This research was supported by startup funds from the Departments of Pathology (BEB), and and utilized the following shared resources: Laboratory Animal Shared Resource (LASR), Translational Imaging Shared Resource (TISR) and Gene Targeting & Transgenic Shared Resource (GeTT) at Roswell Park supported by National Cancer Institute (NCI) Grant (P30CA016056). The authors would like to thank Mr. Steve Turowski (TISR) and the technical staff within the shared resources for their assistance in performing the studies.

References

1. Constantino BT. Red cell distribution width, revisited. *Lab Med.* 2013;44(2):e2-e9.
2. Lippi G, et al. Red Blood Cell Distribution Width Is Significantly Associated With Aging and Gender. *Clin Chem Lab Med.* 2014;52(9):e197-e9.
3. Patel KV, et al. Red blood cell distribution width and the risk of death in middle-aged and older adults. *Arch Intern Med.* 2009;169(5):515-23.
4. Perlstein TS, et al. Red blood cell distribution width and mortality risk in a community-based prospective cohort. *Arch Intern Med.* 2009;169(6):588-94.
5. Felker GM, et al. Red cell distribution width as a novel prognostic marker in heart failure: data from the CHARM Program and the Duke Databank. *J Am Coll Cardiol.* 2007;50(1):40-7.
6. Allen LA, et al. Validation and potential mechanisms of red cell distribution width as a prognostic marker in heart failure. *J Card Fail.* 2010;16(3):230-8.
7. Dabbah S, et al. Relation between red cell distribution width and clinical outcomes after acute myocardial infarction. *Am J Cardiol.*2010;105(3):312-7.
8. Ye Z, et al. Usefulness of red cell distribution width to predict mortality in patients with peripheral artery disease. *Am J Cardiol.* 2011;107(8):1241-5.
9. Montagnana M, and Danese E. Red cell distribution width and cancer. *Ann Transl Med.* 2016;4(20).
10. Hampole CV, et al. Usefulness of red cell distribution width as a prognostic marker in pulmonary hypertension. *Am J Cardiol.* 2009;104(6):868-72.
11. Zorlu A, et al. Usefulness of admission red cell distribution width as a predictor of early mortality in patients with acute pulmonary embolism. *Am J Cardiol.* 2012;109(1):128-34.
12. Lee JH, et al. Red cell distribution width as a prognostic marker in patients with community-acquired pneumonia. *Am J Emerg Med.* 2013;31(1):72-9.
13. Braun E, et al. Elevated red cell distribution width predicts poor outcome in young patients with community acquired pneumonia. *Crit Care.* 2011;15(4):1-9.
14. Foy BH, et al. Association of red blood cell distribution width with mortality risk in hospitalized adults with SARS-CoV-2 infection. *JAMA Network Open.* 2020;3(9):e2022058-e.
15. Seyhan EC, et al. Red blood cell distribution and survival in patients with chronic obstructive pulmonary disease. *COPD: J Chronic Obstr Pulm Dis.* 2013;10(4):416-24.

16. Epstein D, et al. Increased red cell distribution width: A novel predictor of adverse outcome in patients hospitalized due to acute exacerbation of chronic obstructive pulmonary disease. *Respir Med.* 2018;136:1-7.
17. Wang B, et al. Relation between red cell distribution width and mortality in critically ill patients with acute respiratory distress syndrome. *BioMed Res Int.* 2019; 2019:1942078.
18. Kim J, et al. Red blood cell distribution width is associated with poor clinical outcome in acute cerebral infarction. *Thromb Haemost.* 2012;108(08):349-56.
19. Ani C, and Ovbiagele B. Elevated red blood cell distribution width predicts mortality in persons with known stroke. *J Neurol Sci.* 2009;277(1-2):103-8.
20. Wang F, et al. Red cell distribution width as a novel predictor of mortality in ICU patients. *Ann Med.* 2011;43(1):40-6.
21. Bazick HS, et al. Red Cell Distribution Width and all cause mortality in critically ill patients. *Crit Care Med.* 2011;39(8):1913.
22. Majercik S, et al. Red cell distribution width is predictive of mortality in trauma patients. *J Trauma Acute Care Surg.* 2013;74(4):1021-6.
23. Garbharran U, et al. Red cell distribution width is an independent predictor of mortality in hip fracture. *Age Ageing.* 2013;42(2):258-61.
24. Jo YH, et al. Red cell distribution width is a prognostic factor in severe sepsis and septic shock. *Am J Emerg Med.* 2013;31(3):545-8.
25. Ku NS, et al. Red blood cell distribution width is an independent predictor of mortality in patients with gram-negative bacteremia. *Shock.* 2012;38(2):123-7.
26. Şenol K, et al. Red cell distribution width as a predictor of mortality in acute pancreatitis. *Am J Emerg Med.* 2013;31(4):687-9.
27. Vashistha T, et al. Red cell distribution width and mortality in hemodialysis patients. *Am J Kidney Dis.* 2016;68(1):110-21.
28. Mucsi I, et al. Red cell distribution width is associated with mortality in kidney transplant recipients. *Int Urol Nephrol.* 2014;46(3):641-51.
29. Cavusoglu E, et al. Relation between red blood cell distribution width (RDW) and all-cause mortality at two years in an unselected population referred for coronary angiography. *Int J Cardiol.* 2010;141(2):141-6.
30. Uyarel H, et al. Red cell distribution width as a novel prognostic marker in patients undergoing primary angioplasty for acute myocardial infarction. *Coron Artery Dis.* 2011;22(3):138-44.

31. Lam AP, et al. Multiplicative interaction between mean corpuscular volume and red cell distribution width in predicting mortality of elderly patients with and without anemia. *Am J Hematol.* 2013;88(11):E245-E9.
32. Núñez J, et al. Red blood cell distribution width is longitudinally associated with mortality and anemia in heart failure patients. *Circulation J.* 2014;78(2):410-8.
33. Lv H, et al. Red cell distribution width as an independent predictor of long-term mortality in hip fracture patients: a prospective cohort study. *J Bone Miner Res.* 2016;31(1):223-33.
34. Shah N, et al. Red cell distribution width and risk of cardiovascular mortality: Insights from National Health and Nutrition Examination Survey (NHANES)-III. *Int J Cardiol.* 2017;232:105-10.
35. Patel KV, et al. Red cell distribution width and mortality in older adults: a meta-analysis. *J Gerontol A Biol Sci Med Sci.* 2009;65(3):258-65.
36. Lippi G, et al. Relation between red blood cell distribution width and inflammatory biomarkers in a large cohort of unselected outpatients. *Arch Pathol Lab Med.* 2009;133(4):628-32.
37. Emans ME, et al. Red cell distribution width is associated with physical inactivity and heart failure, independent of established risk factors, inflammation or iron metabolism; the EPIC—Norfolk study. *Int J Cardiol.* 2013;168(4):3550-5.
38. Lappé JM, et al. Red cell distribution width, C-reactive protein, the complete blood count, and mortality in patients with coronary disease and a normal comparison population. *Clin Chim Acta.* 2011;412(23-24):2094-9.
39. Patel KV, et al. *Oxygen Transport to Tissue XXXIV*. Springer; 2013:211-6.
40. Vayá A, et al. Red blood cell distribution width and erythrocyte deformability in patients with acute myocardial infarction. *Clin Hemorheol Microcirc.* 2015;59(2):107-14.
41. Sun H, and Weaver CM. Decreased Iron Intake Parallels Rising Iron Deficiency Anemia and Related Mortality Rates in the US Population. *J Nutr.* 2021.
42. Yčas JW, et al. Persistent increase in red cell size distribution width after acute diseases: A biomarker of hypoxemia? *Clin Chim Acta.* 2015;448:107-17.
43. Tertemiz KC, et al. Could "red cell distribution width" predict COPD severity? Rev Port Pneumo *(English Edition).* 2016;22(4):196-201.
44. Karampitsakos T, et al. The role of increased red cell distribution width as a negative prognostic marker in patients with COPD. *Pulm Pharmacol Ther.* 2020;60:101877.
45. Grant BJ, et al. Relation between lung function and RBC distribution width in a population-based study. *Chest.* 2003;124(2):494-500.

46. Thayer TE, et al. Unbiased Phenome-Wide Association Studies of Red Cell Distribution Width Identifies Key Associations with Pulmonary Hypertension. *Ann Am Thorac Soc.* 2019;16(5):589-98.
47. Xie J, et al. Association between hypoxemia and mortality in patients with COVID-19. *Mayo Clin Proc.* 2020;95(6):1138-47.
48. Franke K, et al. Erythrocytosis: the HIF pathway in control. *Blood, The Journal of the American Society of Hematology.* 2013;122(7):1122-8.
49. Favier J, et al. Paraganglioma and phaeochromocytoma: from genetics to personalized medicine. *Nat Rev Endocrinol.* 2015;11(2):101-11.
50. Baysal BE, et al. Mutations in SDHD, a mitochondrial complex II gene, in hereditary paraganglioma. *Science (New York, NY).* 2000;287(5454):848-51.
51. Rodriguez-Cuevas H, et al. High-altitude paragangliomas diagnostic and therapeutic considerations. *Cancer.* 1986;57(3):672-6.
52. Astrom K, et al. Altitude is a phenotypic modifier in hereditary paraganglioma type 1: evidence for an oxygen-sensing defect. *Hum Genet.* 2003;113(3):228-37.
53. Cerecer-Gil NY, et al. Mutation of SDHB is a cause of hypoxia-related high-altitude paraganglioma. *Clin Cancer Res.* 2010;16(16):4148-54.
54. Castro-Vega LJ, et al. Multi-omics analysis defines core genomic alterations in pheochromocytomas and paragangliomas. *Nat Commun.* 2015;6(1):1-9.
55. Piruat JI, and Millán-Uclés Á. Genetically modeled mice with mutations in mitochondrial metabolic enzymes for the study of cancer. *Front Oncol.* 2014;4:200.
56. Khazal FA, et al. A conditional mouse model of complex II deficiency manifesting as Leigh-like syndrome. *The FASEB Journal.* 2019;33(12):13189-201.
57. Al Khazal F, et al. Unexpected obesity, rather than tumorigenesis, in a conditional mouse model of mitochondrial complex II deficiency. *The FASEB Journal.* 2021;35(2):e21227.
58. Sharma S, et al. Mitochondrial complex II regulates a distinct oxygen sensing mechanism in monocytes. *Hum Mol Genet.* 2017;26(7):1328-39.
59. Oudijk L, et al. The role of immunohistochemistry and molecular analysis of succinate dehydrogenase in the diagnosis of endocrine and non-endocrine tumors and related syndromes. *Endocr Pathol.* 2019;30(1):64-73.
60. Saldana MJ, et al. High altitude hypoxia and chemodectomas. *Hum Pathol.* 1973;4(2):251-63.

61. Motulsky HJ, and Brown RE. Detecting outliers when fitting data with nonlinear regression–a new method based on robust nonlinear regression and the false discovery rate. *BMC Bioinform.* 2006;7(1):1-20.
62. Kita K, et al. Role of complex II in anaerobic respiration of the parasite mitochondria from Ascaris suum and Plasmodium falciparum. *Biochim Biophys Acta Bioenerg.* 2002;1553(1-2):123-39.
63. Hartman T, et al. Succinate dehydrogenase is the regulator of respiration in Mycobacterium tuberculosis. *PLoS Pathog.* 2014;10(11):e1004510.
64. Müller M, et al. Biochemistry and evolution of anaerobic energy metabolism in eukaryotes. *Microbiol Mol Biol Rev.* 2012;76(2):444-95.
65. Ali SS, et al. Hypoxia-adaptation involves mitochondrial metabolic depression and decreased ROS leakage. *PloS one.* 2012;7(5):e36801.
66. Eprintsev AT, et al. Expression and promoter methylation of succinate dehydrogenase and fumarase genes in maize under anoxic conditions. *J Plant Physiol.* 2017;216:197-201.
67. Yao Q, et al. Suppressing mitochondrial respiration is critical for hypoxia tolerance in the fetal growth plate. *Dev. Cell* 2019;49(5):748-63. e7.
68. Selak MA, et al. Succinate links TCA cycle dysfunction to oncogenesis by inhibiting HIF-alpha prolyl hydroxylase. *Cancer cell.* 2005;7(1):77-85.
69. Smith EH, et al. Succinate inhibition of alpha-ketoglutarate-dependent enzymes in a yeast model of paraganglioma. *Hum Mol Genet.* 2007;16(24):3136-48.
70. Letouzé E, et al. SDH mutations establish a hypermethylator phenotype in paraganglioma. *Cancer cell.* 2013;23(6):739-52.
71. Baysal BE. Genomic imprinting and environment in hereditary paraganglioma. *Am J Med Genet C Semin Med Genet.* 2004;129C(1):85-90.
72. Sharma S, et al. Mitochondrial hypoxic stress induces widespread RNA editing by APOBEC3G in natural killer cells. *Genome Biol.* 2019;20(1):37-019-1651-1.
73. Sharma S, et al. APOBEC3A cytidine deaminase induces RNA editing in monocytes and macrophages. *Nat Commun.* 2015;6(1):1-15.
74. Baysal BE, et al. Hypoxia-inducible C-to-U coding RNA editing downregulates SDHB in monocytes. *PeerJ.* 2013;1:e152.
75. Lin X, et al. A chemical genomics screen highlights the essential role of mitochondria in HIF-1 regulation. *Proc Natl Acad Sci U S A.* 2008;105(1):174-9.
76. Taylor CT. Mitochondria and cellular oxygen sensing in the HIF pathway. *Biochem J.* 2008;409(1):19-26.

77. Quinlan CL, et al. Mitochondrial complex II can generate reactive oxygen species at high rates in both the forward and reverse reactions. *J Biol Chem.* 2012;287(32):27255-64.
78. Miyadera H, et al. Atpenins, potent and specific inhibitors of mitochondrial complex II (succinate-ubiquinone oxidoreductase). *Proc Natl Acad Sci U S A.* 2003;100(2):473-7.
79. Wang H, et al. Synthesis and antineoplastic evaluation of mitochondrial complex II (succinate dehydrogenase) inhibitors derived from atpenin A5. *ChemMedChem.* 2017;12(13):1033-44.
80. Jain IH, et al. Hypoxia as a therapy for mitochondrial disease. *Science.* 2016;352(6281):54-61.
81. Piruat JI, et al. The mitochondrial SDHD gene is required for early embryogenesis, and its partial deficiency results in persistent carotid body glomus cell activation with full responsiveness to hypoxia. *Mol Cell Biol.* 2004;24(24):10933-40.
82. Sharma R, et al. Influence of the implantation site on the sensitivity of patient pancreatic tumor xenografts to Apo2L/TRAIL therapy. *Pancreas.* 2014;43(2):298.
83. Ito F, et al. Water: a simple solution for tumor spillage. *Ann Surg Oncol.* 2011;18(8):2357-63.
84. Chen WW, et al. Absolute quantification of matrix metabolites reveals the dynamics of mitochondrial metabolism. *Cell.* 2016;166(5):1324-37. e11.
85. Simon-Manso Y, et al. Metabolite profiling of a NIST Standard Reference Material for human plasma (SRM 1950): GC-MS, LC-MS, NMR, and clinical laboratory analyses, libraries, and web-based resources. *Anal Chem.* 2013;85(24):11725-31.
86. Smith CA, et al. METLIN: a metabolite mass spectral database. *Ther Drug Monit.* 2005;27(6):747-51.
87. Jones E, et al. SciPy: Open source scientific tools for Python. 2001.
88. Kolde R. pheatmap: Pretty Heatmaps. R package version 1.0. 8. 2015.

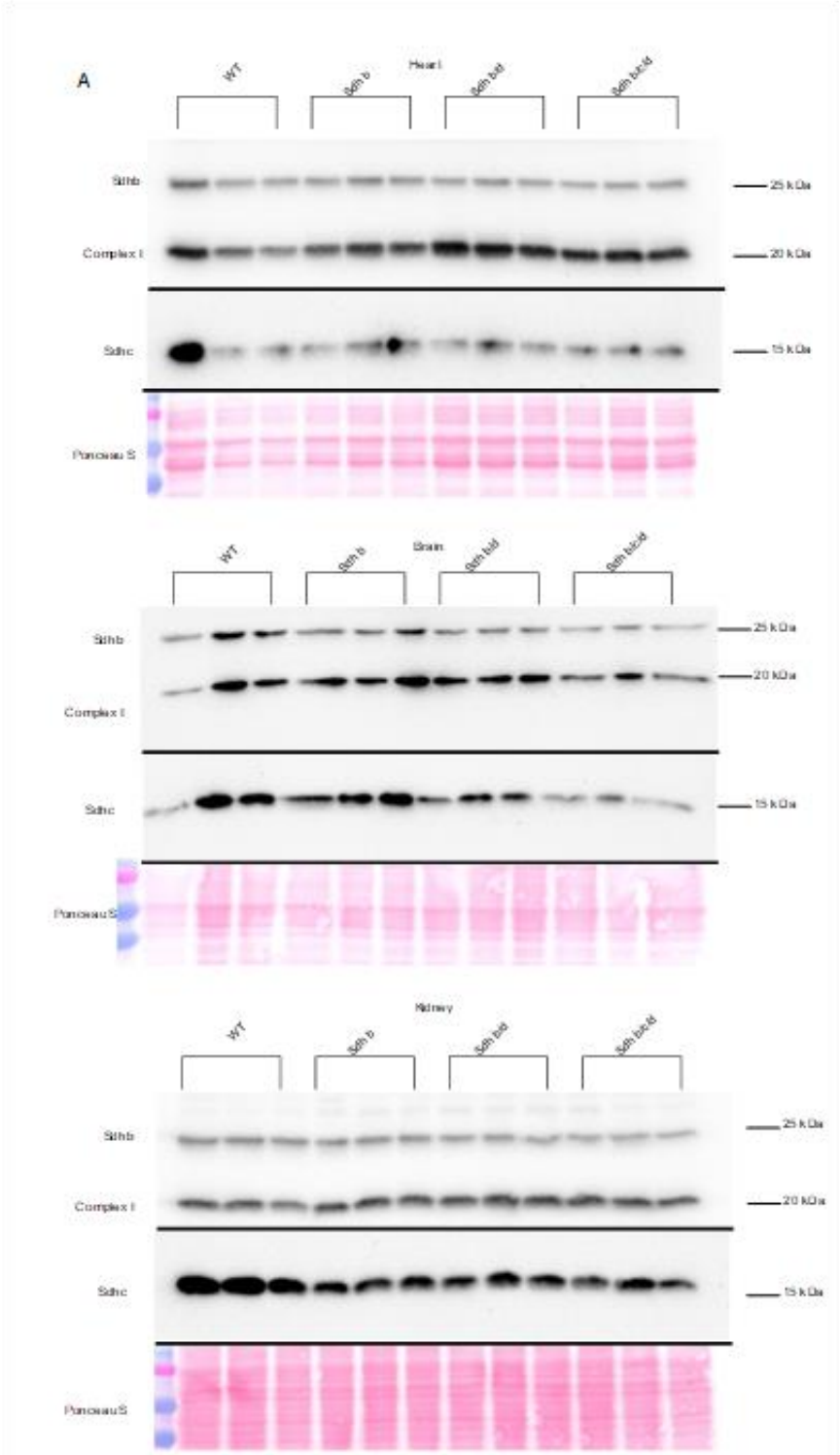

Figure 1A. **Protein levels of succinate dehydrogenases decrease in Sdh chKO mice. (A)** Western blots of Sdhb, Sdhc and Complex I protein NDUFB8 from heart, kidney and brain tissues from WT (n=3), Sdhb (n=3), Sdhb/d (n=3) and Sdhb/c/d (n=3) mice. Ponceau S staining was used as a loading control. The experiment is conducted once.

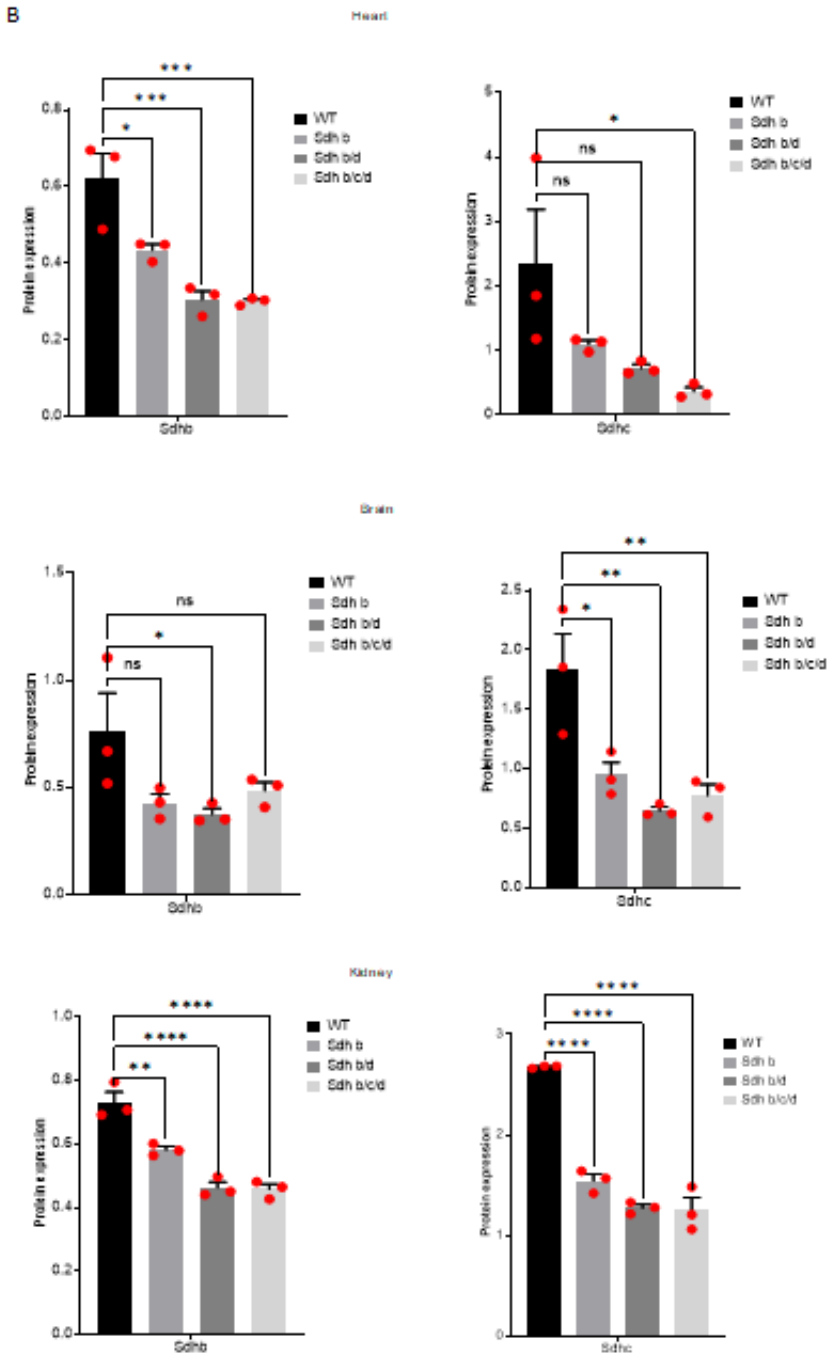

Figure 1B. **Protein levels of succinate dehydrogenases decrease in Sdh chKO mice. (B)** Quantification of bands intensity as a measurement of protein levels from heart, kidney and brain tissues from WT (n=3), Sdhb (n=3), Sdhb/d (n=3) and Sdhb/c/d (n=3) mice. Sdhb and Sdhc were normalized to Complex I NDUFB8. P values are calculated by ordinary one-way ANOVA, (* P< 0.05, **P<0.01, ***P<0.001, ****P<0.0001). Data represent mean ± SEM.

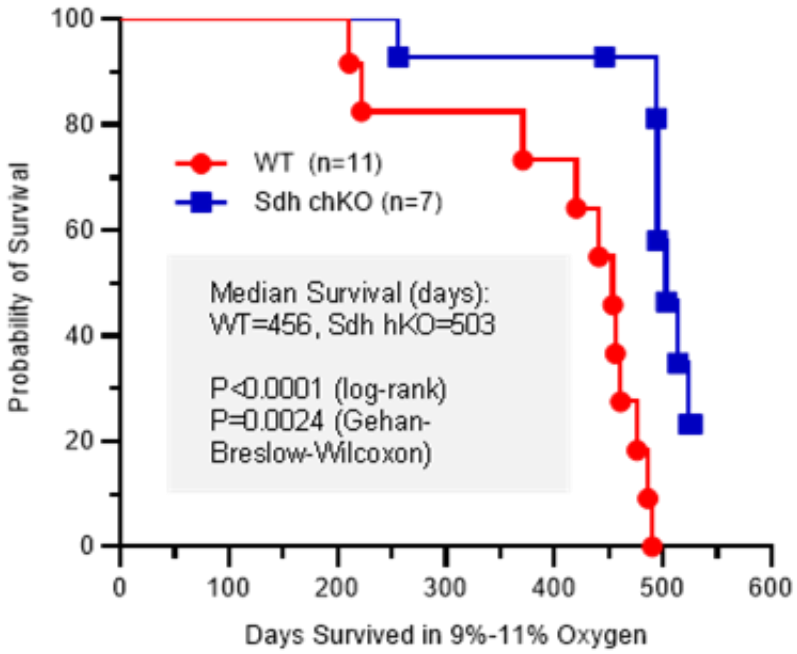

Figure 2 . Kaplan-Meier healthy lifespan analysis of WT and Sdh chKO male mice from 3 groups. The curve differences (n=15 WT and n=15 chKO) are statistically significant by Log-rank (Mantel-Cox) and Gehan-Breslow-Wilcoxon tests. Healthy lifespan is measured by the total number of days until spontaneous death or the development of morbidities that require euthanasia in chronic hypoxia. The depicted curve includes all mice that died spontaneously or euthanized due to morbidity (e.g. all events described in Table 1). The curve excludes points for four WT, which include M197 and 3 mice from experiment#3 (Table 1), and eight chKO, which include M145, M515, M536 and 5 mice from experiment#3 (Table 1). These mice are censored since they did not complete the lifespan end points.

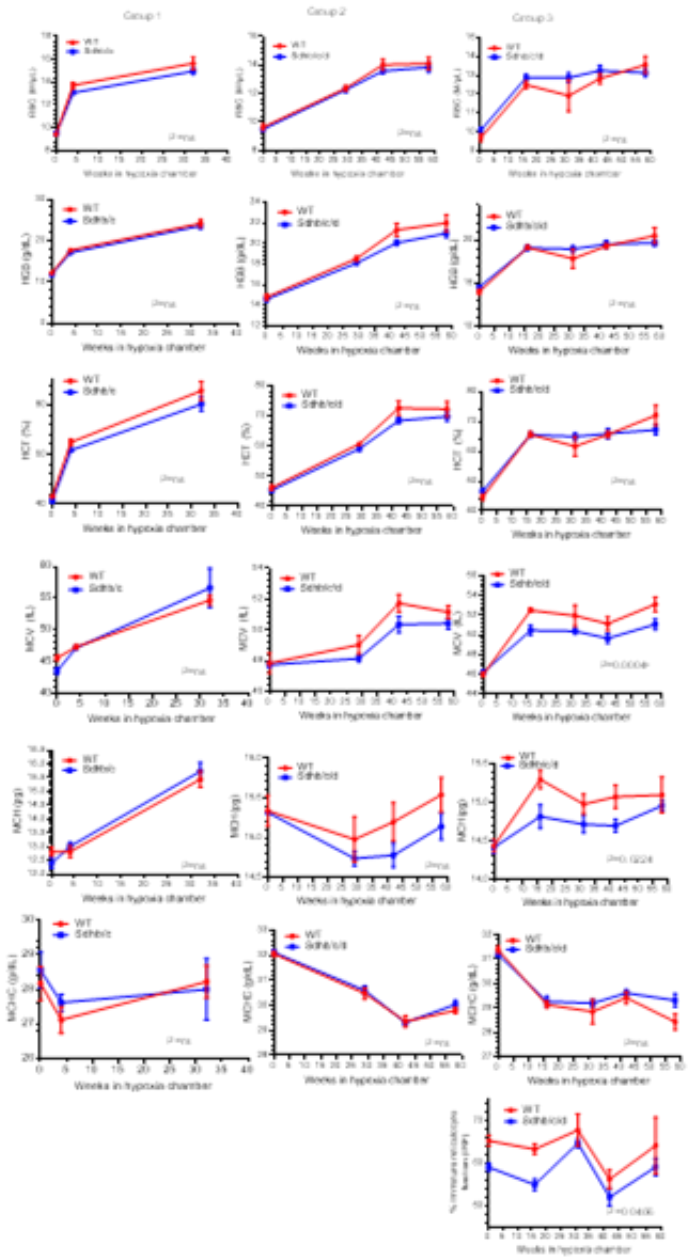

Figure 3. RBC, HGB, HCT, MCV, MCH, MCHC and IRF in Sdh chKO (Sdhb/c in Group 1 and Sdhb/c/d in Groups 2 and 3) and WT control mice under chronic hypoxia. RBC numbers, hemoglobin (HGB) and hematocrit (HCT), mean corpuscle volume (MCV), mean corpuscle hemoglobin (MCH), mean corpuscle hemoglobin concentration (MCHC) and and immature reticulocyte fraction (IRF) are shown. Each time point contains 3-5 male mice and shows mean and SEM. P values are calculated by 2way ANOVA using time and genotype as independent variables. [A]P value remains significant (less than 0.05) after adjustment for multiple comparisons by Holm-Šídák method (alpha:0.05). The missing parameter IRF in Groups 1 and 2 were not available in earlier CBC outputs. (HGB results of Groups 1 and 2 were previously shown in Sharma et al. (58), and included here for comprehensive analysis.)

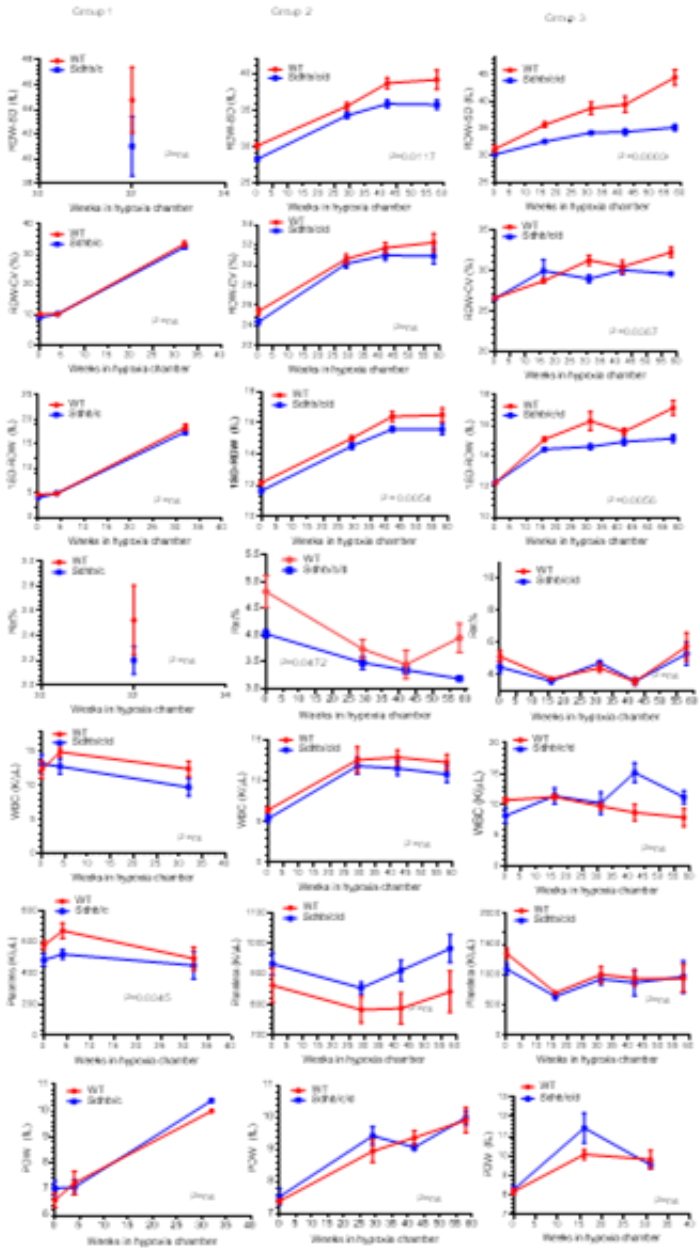

Figure 4. RDW-SD, RDW-CV, 1SD-RDW, Ret%, WBC, platelets and PDW in Sdh chKO (Sdhb/c in Group 1 and Sdhb/c/d in Groups 2 and 3) and WT control mice under chronic hypoxia. Measures of RBC size variation including RDW-SD, RDW-CV and 1 standard deviation of RDW (1SD-RDW), reticulocyte percentage (Ret%) , white blood cell (WBC), plateletsand platelet distribution width (PDW) are shown. Each time point contains 3-5 male mice and shows mean and SEM. P values are calculated by 2way ANOVA using time and genotype as independent variables. [A]P value remains significant (less than 0.05) after adjustment for multiple comparisons by Holm-Šídák method (alpha:0.05). The missing parameters in Group 1 (RDW-SD, Ret%) were not available in earlier CBC outputs. The missing parameter IRF in Group 1 and 2 were not available in earlier CBC outputs.

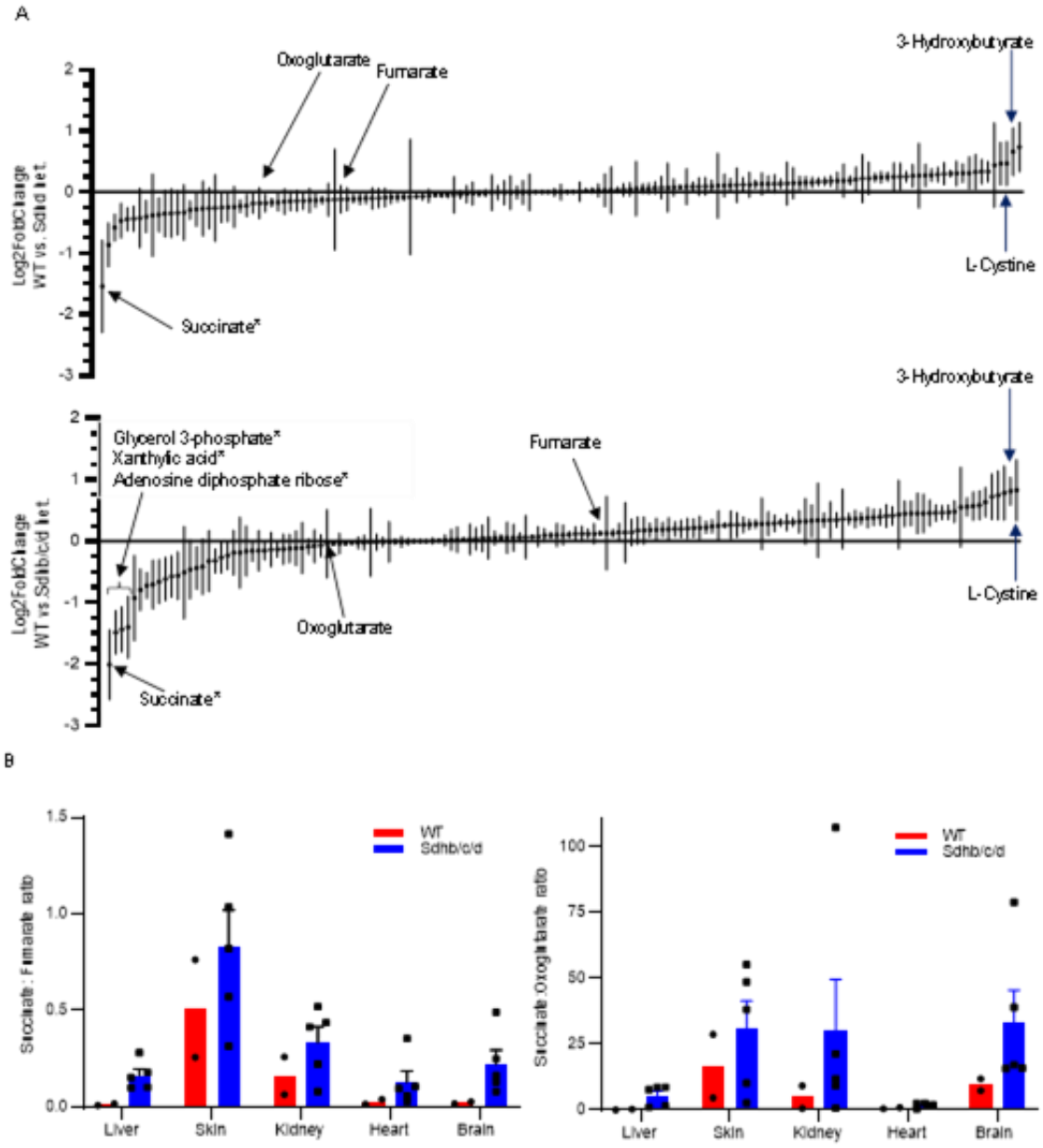

Figure 5. Metabolite profiling in WT vs. Sdh hKO mice under normoxic conditions. (A) Average fold-changes (log2FoldChange) of liver, heart, kidney, skin and brain in 147 metabolites are ranked. Both Sdhd single hKO (n=3) and Sdhb/c/d triple hKO mice (n=5) tissues showed the highest increase in succinate, and the highest overlapping decreases in 3-hydroxybutyrate and L-Cystine relative to WT control mice (n=2). A stringent outlier analysis by ROUT method (Q=0.1%) detected only four outlier metabolites marked by asterisk. **(B)** The ratios of succinate to fumarate and oxoglutarate were increased in Sdhb/c/d hKO mice relative to WT. Data represent mean ± SEM.

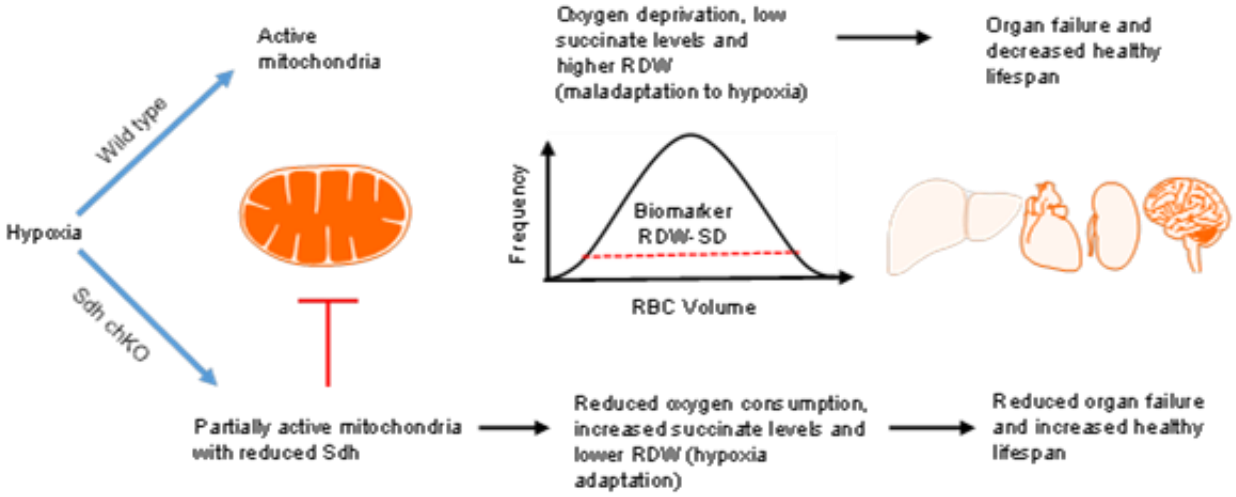

Figure 6. **A mitochondrial basis for the association between high RDW and mortality in hypoxia.** When oxygen is limited, fully active mitochondria exhausts the remaining oxygen leading to oxygen deprivation, erythrocyte regeneration, high RDW, compromised cellular viability, organ failure and mortality. Inhibition of Sdh reduces oxygen consumption and RDW levels, and triggers cellular hypoxia adaptation pathways leading to improved survival.

Table 1

Lifespan of mice under chronic hypobaric hypoxia

Group no. (start date)	Mouse ID	Genotype	Survival time (days)	Manner of death	Euthanasia indication
1 (03/25/13)	M194	WT	461	Spontaneous	-
	M195	WT	441	Spontaneous	-
	M196	WT	211	Spontaneous	-
	M197	WT	211	Euthanasia	Elective for tumor evaluation
	M198	WT	420	Spontaneous	-
	M145	Sdhb/c	211	Euthanasia	Elective for tumor evaluation
	M146	Sdhb/c	494	Euthanasia	Moribund
	M147	Sdhb/c	514	Spontaneous	-
	M148	Sdhb/c	256	Spontaneous	-
	M185	Sdhb/c	503	Spontaneous	-
2 (06/09/15)	M598	WT	476	Euthanasia	Moribund#
	M599	WT	490	Spontaneous	-
	M600	WT	486	Euthanasia	Moribund#
	M601	WT	454	Spontaneous	-
	M602	WT	456	Spontaneous	-
	M515	Sdhb/c/d	527	Euthanasia	Elective^
	M518	Sdhb/c/d	495	Spontaneous	-

	M527	Sdhb/c/d	495	Spontaneous	-
	M531	Sdhb/c/d	524	Spontaneous	-
	M536	Sdhb/c/d	527	Euthanasia	Elective^
3 (08/18/17)*	M773	WT	371	Euthanasia	Weight loss, rectal prolapse
	M803	WT	222	Euthanasia	Rectal prolapse

^M515 and M536 were the last surviving mice in group 2, and euthanized electively. #M598 and M600 showed limited spontaneous mobility (videos available). *The experiment with Group 3 is stopped on day 446, when there were 3 WT and 5 Sdhb/c/d alive, due to hypoxia chamber failure. These and the four electively euthanized mice are censored in Kaplan Meier survival analysis.

Table 2

Comparison of RBC parameters between Sdh chKO and WT male mice in baseline normoxia and chronic hypobaric hypoxia

Parameter	Normoxia (P values)	Hypoxia (P values)
RBC (million/µL)	ns	ns
HGB (g/dL)	ns	ns
HCT (%)	ns	0.0332
MCV (fL)	ns	ns
MCH (pg)	ns	0.0467
MCHC (g/dL)	ns	ns
RDW-SD (fL)	0.0022[A]	<0.0001[A]
RDW-CV (%)	0.0038[A]	0.0006[A]
1SD-RDW (fL)	0.0042[A]	<0.0001[A]
Ret%	0.0216	ns
Immature reticulocyte fraction (IRF)	0.0159	ns
WBC (K/µL)	ns	ns
Platelets (K/µL)	ns	ns
PDW (fL)	ns	ns

P values are obtained by 2way ANOVA comparing Sdh KO vs. WT mice combining data from all time points from groups 1, 2 and 3. IRF data were available from group 3 only, and its P value is obtained by Mann-Whitney test, two-tailed. [A]These P values remain significant (less than 0.05) after adjustment for multiple comparisons by Holm-Šídák method (alpha:0.05).